

Journal of Materials Chemistry A

Accepted Manuscript



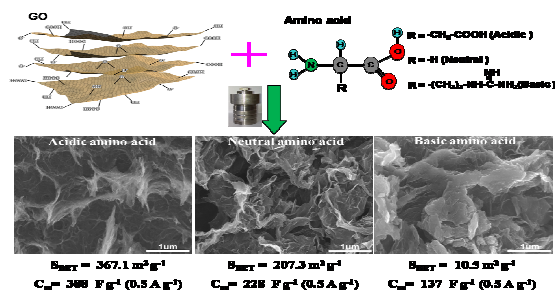
This is an *Accepted Manuscript*, which has been through the Royal Society of Chemistry peer review process and has been accepted for publication.

Accepted Manuscripts are published online shortly after acceptance, before technical editing, formatting and proof reading. Using this free service, authors can make their results available to the community, in citable form, before we publish the edited article. We will replace this *Accepted Manuscript* with the edited and formatted *Advance Article* as soon as it is available.

You can find more information about *Accepted Manuscripts* in the [Information for Authors](#).

Please note that technical editing may introduce minor changes to the text and/or graphics, which may alter content. The journal's standard [Terms & Conditions](#) and the [Ethical guidelines](#) still apply. In no event shall the Royal Society of Chemistry be held responsible for any errors or omissions in this *Accepted Manuscript* or any consequences arising from the use of any information it contains.

Table of contents



Nitrogen-doped graphene were synthesized using amino acid as doping agent. The acidity of amino acid affect the morphology, and ultimately affect the electrochemical performance of NG.

Cite this: DOI: 10.1039/c0xx00000x

paper

www.rsc.org/xxxxxx

Hydrothermal synthesis of nitrogen-doped graphene hydrogel using amino acid with different acidities as doping agent

Tao wang^a, Luxiang Wang^a, Dongling Wu^a, Wei Xia^b, Hongyang Zhao^a and Dianzeng Jia^{*a}

A one-pot hydrothermal route was developed for the preparation of nitrogen-doped graphene (NG) hydrogel using graphene oxide (GO) as raw material and nine amino acids with different acidities (acidic, neutral and basic) as doping agents. The morphology, structure and composition of the prepared NG using three amino acids (DL-aspartic acid, acidic; L-glycine, neutral; L-arginine, basic.) were characterized by SEM, Nitrogen physisorption, Raman and XPS spectroscopy. Acidic amino acid yielded NG with cross-linked 3D network with a large specific surface area of 367.1 m² g⁻¹, while NG with basic amino acid showed a tightly stacked structure with a much smaller surface area of 10.5 m² g⁻¹. The charged amino acid, and the ensuing electrostatic interactions between amino acid and GO affect the morphology of NG, and ultimately affect its electrochemical performance. The sample prepared using acidic amino acid, with the lowest surface N content (1.0 %) but the largest surface area displayed high specific capacitance of 246 F g⁻¹ at 3 A g⁻¹. The microstructure, surface area and effective nitrogen content, mainly the pyridinic nitrogen group related to pseudocapacitance, play important roles in the capacitive performance of the NG samples.

1. Introduction

Graphene, with two-dimensional (2D) structure, has emerged as one of the most active research fields because of its remarkable electronic, thermal and mechanical properties.¹ Some of the most promising applications of graphene are related to its electronic properties. Thus, tremendous efforts have been made in the last few years to tune the electronic properties of graphene, for example, by controlling its crystal structure or chemical doping with guest atoms. Chemical doping with heteroatoms has proved to be highly effective in the doping of other carbon materials like carbon nanotubes, which extended the diversity of their applications.² Among others, nitrogen, sulfur, phosphorus and boron are the most commonly used dopants for the doping of graphene.³⁻⁵ Especially, nitrogen is considered to be the ideal dopant for graphene because of its comparable atomic size to carbon and high electronegativity.⁶⁻⁸

The synthesis of nitrogen-doped graphene has been achieved via a variety of pathways, such as arc-discharge,⁹ nitrogen plasma process,^{10,11} chemical vapor deposition (CVD),^{12,13} segregation growth,¹⁴ or thermal (or electrical) annealing post treatment.^{15,16} Recently, hydrothermal reaction method has been used as an effective approach to fabricate graphene hydrogel¹⁷ and nitrogen-doped graphene (NG) hydrogel.^{4,18-22} Various nitrogen sources have been reported so far using hydrothermal method, such as pyrrole⁴, ammonia¹⁸ or organic amine,¹⁹⁻²¹ urea,²²⁻²⁴ hydrazine hydrate.²⁵ However, environmental and toxicity concerns related to most of the nitrogen sources motivate us to find more environment-friendly ones.

Amino acid as a low cost and green material contains multifunctional groups (-NH₂, -COOH and other functional groups) and has been applied in the synthesis of doped carbon materials²⁶⁻³⁰. Recently, Chen et al.³¹ employed L-cysteine as a reductant to prepare of reduced graphene oxide (RGO) nanosheets at room temperature. However, to our knowledge, using amino acid as nitrogen source for the synthesis of NG has not been reported so far.

The pH plays an important role in the morphology, structure and electrochemical properties of RGO during the hydrothermal reduction of GO.³²⁻³⁴ Navarro et al.³⁴ concluded that acidic conditions lead to a higher amount of defects in the resulting RGO samples with smaller sizes of the sheets and a pronounced tendency of these sheets to aggregate, while more basic conditions promote a decrease in the number of defects present in the resulting RGO and bigger graphitic domains.

Herein, inspired by those works, amino acids, as environment-friendly nitrogen source, were used to synthesize NG via a one-pot hydrothermal method. The NG hydrogels were obtained using GO as raw material, and three amino acids with difference acidities as nitrogen sources, including DL-aspartic acid (acidic), L-glycine (neutral) and L-arginine (basic). The microstructure and nitrogen doping level of the obtained samples were systematically investigated and the performance of NG as free standing electrode in supercapacitors were tested and analyzed. Furthermore, six additional amino acids were selected to synthesize NG hydrogels. The influence of synthesis conditions on the morphology and subsequently the electrochemical performance of NG samples were investigated including the acidity of amino acid and the pH of the solution.

2. Experimental section

Materials

Graphite powder (8000 mesh, 99.95%, metals basis) was purchased from Aladdin-reagent. Co., Ltd (Shanghai, China). Amino acids (purity: 98%) were purchased from Shanghai Lanji Technology Development Ltd. Analytical-grade KMnO_4 , KOH , 85% H_3PO_4 , 98% H_2SO_4 , 36% HCl and 30% H_2O_2 aqueous solution were purchased from Beijing Chemical Reagents Company. All reagents were used directly without further purification, and the water used in the experiments was freshly deionized.

Preparation of GO

Improved Hummers' method was used in the synthesis,³⁵ that is, a mixture of concentrated $\text{H}_2\text{SO}_4/\text{H}_3\text{PO}_4$ (360:40 mL) was added to a mixture of graphite flakes (3.0g, 1wt equiv.) and KMnO_4 (18.0g, 6wt equiv.), which resulted in a slightly exothermic reaction increasing the temperature to 35–40°C. The reaction mixture was then heated to 50°C and stirred for 12h. Subsequently, the reaction was cooled to room temperature and poured onto ice (~400 mL) with 30% H_2O_2 (5 mL) and 30% HCl (200 mL). For the workup, the filtrate was centrifuged (10000 rpm for 30 min), and the supernatant was decanted. The mixture was filtered followed by repeated washing of the solid product with deionized water and centrifugation to remove metal ion and acid until the pH of the filtrate reached 7.

Preparation of NG

The obtained GO were used as raw material for the synthesis of NG. Nine different amino acids with different acidities, i.e., DL-Aspartic Acid (acidic), L-Glutamic Acid (acidic), L-Leucine (neutral), L-Alanine (neutral), L-Threonine (neutral), L-Glycine (neutral), L-Lysine (basic), L-Histidine (basic) and L-Arginine (basic) were applied as doping agents. After initial tests with these amino acids, three of them were selected for detailed investigations representing different acidities as shown in Fig. 1a. In a typical synthesis, a 2 mg mL^{-1} solution of graphitic oxide in deionized water was bath-sonicated for 1 h to give a brown colloidal solution. Then, 0.15 g amino acids were dissolved in 30 mL of 2 mg mL^{-1} of aqueous GO solution (the mass ratio of amino acid to GO is 2.5:1). The mixture was magnetically stirred for 10 minutes, transferred to a Teflon-lined autoclave and subjected to hydrothermal treatment for 3 h at 160°C. After that, the autoclave was naturally cooled to room temperature and the as prepared NG hydrogels were removed from the autoclave and immersed in deionized water for seven days, during which deionized water was renewed once a day to remove any unreacted reagent. Subsequently, the NG hydrogels were freeze-dried under vacuum for further characterization. After freeze-drying, the obtained samples were labeled as NGasp for DL-aspartic acid, NGgly for L-glycine, and NGarg for L-arginine. For comparison, RGO was prepared by the same method in the absence of amino acid. The water content of the NG (W_w , wt%) was calculated by $W_w = (W_t - W_d)/W_t \times 100$, where W_t is the total weight of the NG and W_d is the weight of the NG in the dry state. Additionally, NGasp samples of mass ratios of 1:1 and 10:1 were also prepared by the same process, and were labeled as NGasp1 and NGasp10, respectively. Extensive experimental characterization details of

NGasp1 and NGasp10 are provided with the Supporting Information. FTIR spectroscopy was employed to investigate the purity of the products after purification (for details, see FT-IR characterization and Fig. S1‡ in Supporting Information).

Characterization

Morphology of the synthesized materials were investigated by scanning electron microscopy (SEM, Hitachi S-4800) with an acceleration voltage of 5 kV. X-ray diffraction (XRD) measurements were conducted using a D8 (Bruker) X-ray diffractometer with $\text{Cu K}\alpha$ radiation ($\lambda=1.5418 \text{ \AA}$). X-ray photoelectron spectroscopic (XPS) measurements were obtained with an ESCALab220i-XL electron spectrometer from VG Scientific using 300W $\text{Al K}\alpha$ radiation. The base pressure was about 1×10^{-9} mbar and the binding energies were referenced to the C1s line at 284.8 eV from adventitious carbon. A Shirley-type background was subtracted from each spectrum and Avantage 4.15 software was used for curve-fitting. Raman spectroscopy were recorded using a BRUKER VERTEX 70 (532 nm laser) system. Nitrogen physisorption was carried out at 77 K with an ASAP 2050 tended Pressure Sorption Analyzer.

Electrochemical measurements

Electrochemical measurements were performed using a CHI 660D electrochemical workstation (CH Instruments Inc.) at room temperature. The working electrodes were fabricated by RGO or NG in the wet state without using any binder or conducting additives. A slice of wet RGO or NG hydrogel was cut and blotted with a filter paper to remove excess water; then it was pressed onto a nickel foam sheet ($3 \times 1 \text{ cm}$) at 10 MPa for 30 s. The mass loading of active material on each current collector was about 2 mg. In the three-electrode system, the sample was used as the working electrodes, platinum foil as the counter electrode and standard Hg electrode as reference one, and 6.0 M KOH aqueous solution as electrolyte. Cyclic voltammetry and galvanostatic charge–discharge cycling in the potential range of -1.0 to -0.2V was performed at different scan rate and current densities. Electrochemical impedance spectroscopy (EIS) measurements were carried out by applying an alternating current voltage with 5mV amplitude over a frequency range from 0.01 Hz to 100 kHz at the open circuit potential. The mass specific capacitances (C_{sc}) were calculated by using the equations $C_{sc} = (I\Delta t) / (m\Delta V)$, where I is the constant discharge current (A), Δt is the discharging time (s), m is the mass of one electrode (g), and ΔV is the discharge voltage.

3. Results and discussion

It is reported that the restored conjugated structure of GO sheets during hydrothermal reaction can induce partial overlapping or coalescing of flexible graphene sheets via π - π stacking interactions, which can form graphene hydrogel.¹⁷ In this study, RGO and NG hydrogels were prepared by one-step hydrothermal reaction of GO using amino acids with different acidities (Fig. 1a). As shown in Fig. 1b, the apparent sizes of RGO and NG hydrogel are different. The diameter and height of NG hydrogel are larger than that of RGO, implying that the as prepared NG hydrogels can encapsulate more water in the process of self-assembly. The samples of NGarg, NGgly and NGasp hydrogels

contain about 98.6, 97.1 and 96.3 wt% water, respectively. The inset in Fig. 1b shows a typical photo of NG after freeze-drying. The volume shrinkage is likely due to the overlapping of graphene sheets within the self-aggregation during drying process.

The SEM images show that the freeze-dried RGO (Fig. 2a) and NG samples prepared by adding acidic amino acids (Fig. 2b, Fig. S2†a-c) are composed of interconnected 3D porous network, and the pore structure was formed by cross-linking of graphene sheets. The pore sizes ranged from submicrometer to several micrometers. It is believed that the 3D porous network could contribute to the fast adsorption and diffusion of the ions from the electrolyte, which could enhance the electrochemical performance when these samples are used as electrode in supercapacitors. As to NG samples prepared by adding neutral amino acids, the SEM images (Fig. 2c, Fig. S2†d-f) show folded and wrinkled graphene sheets, and not much pores can be observed in the sheets. However, the SEM images (Fig. 2d, Fig. S2†g and h) show that the NG samples obtained by adding basic amino acids consist of randomly crumpled sheets closely associated with each other and form a tightly stacked solid, which suggests that serious agglomeration occurred when basic amino acids were used as doping agents. The different microscopic structure of NG could be attributed to the different electrostatic interaction between amino acids and GO.

To better understand the interaction between different amino acid and GO, three typical amino acid with different acidities (DL-aspartic acid, acidic; L-glycine, neutral; L-arginine, basic) were selected and tested. It is known that each amino acid has its own characteristic isoelectric point (pI), where the net charge on the molecule is zero, and the pI of L-arginine, L-glycine and DL-aspartic acid is 10.76, 5.97 and 2.97 (Table 1), respectively. After mixed GO with different amino acid, the pH value of GO with L-arginine, L-glycine and DL-aspartic acid is 8.4, 4.1 and 3.2 (Table 1), respectively. Obviously the pH value of the mixed solution of DL-aspartic (3.2) is higher than the pI of DL-aspartic (2.97), so DL-aspartic acid is negatively charged in the mixed solution. On the contrary, the pH value of GO with L-arginine (8.4) and with L-glycine (4.1) are lower than the pI of L-arginine (10.76) and L-glycine (5.97). Thus, these two kinds of amino acids are positively charged in mixed solution. It is known that in aqueous solution GO sheets are negatively charged, and in RGO the carboxylic groups cannot be fully reduced resulting in negatively charged RGO.³⁶ Hence, the amino acid with different charged group will interact with GO. Fig. 3a shows the probably interaction between DL-aspartic and GO. First, the negatively charged GO sheets attract $-\text{NH}_3^+$ group through electrostatic attraction, and then the negatively charged groups (COO^-) can repel the negatively charged GO sheets or repel each other, which can enhance the repulsive force between GO layer. The enhanced repulsive force allows consecutive expanding of interlayer space. As a result, the electrostatic repulsion between GO and DL-aspartic can prevent GO flakes from aggregation and coagulation and form the 3D network structures after hydrothermal reaction. However, the negatively charged GO flakes are attracted by the counterions of positively charged L-glycine and L-arginine ($\text{pH} <$

pI) (Fig. 3b, c). The positively charged amino acid neutralizes the negative charge of GO, which weakens the electrostatic repulsion of the GO sheets and narrowed its distance, and ultimately lead to aggregation and coagulation of samples.

Furthermore, the pH values of the mixed solution for the other six amino acids with GO solution were also tested and those values are listed in Table 1. We found that the pH is higher than pI for all the acidic amino acids, and lower than pI for all the neutral and basic amino acids. This means that all the acidic amino acids are negatively charged and all the neutral and basic amino acids are positively charged in the mixed solution. As a result, acidic amino acids enhance the electrostatic repulsion of the GO sheets, which is beneficial for the formation of 3D network structures. On the contrary, neutral and basic amino acids weaken the repulsive force between GO layers, and ultimately lead to the aggregation of samples. The results that amino acids with different acidities can affect the morphology of samples through electrostatic repulsion or attraction interaction are consistent with the fact that as disclosed by SEM studies (Fig. 2 and Fig. S2†).

The results from XRD measurements are summarized in Fig. 4a and Table 2. The diffraction peak located at $2\theta = 9.9^\circ$ can be attributed to the (002) crystalline plane of GO, and the calculated interlayer spacing is about 0.89 nm. The peak at $2\theta = 9.9^\circ$ entirely disappeared after the hydrothermal reaction due to the deoxygenation of oxygen functional groups. After hydrothermal reaction and doping, a broad diffraction peak centered at around 24.7° (d_{002} is 0.360 nm), and 24.5° (d_{002} is 0.363 nm) was observed for RGO and NGasp, respectively. It can be seen that the interlayer spacing of RGO and NGasp are larger than that of graphite (d_{002} is 0.335 nm), indicating the presence of few-layer stacked graphene sheets and the recovery of a graphitic crystal structure.³⁷ Compared with that of NGasp, the (002) peak of NGgly and NGarg show a markedly reduced intensity and dramatically broadened width. The peaks centered at around 29° of the graphite (002) plane were observed for NGgly and NGarg, implying that the interlayer spacing of NGgly and NGarg are smaller than that of NGasp.

Further insights of the structural and electronic properties of graphene were obtained from Raman spectroscopy studies. As shown in Fig. 4b, two remarkable peaks located at around 1346 and 1597 cm^{-1} were observed, which can be attributed to D band associated with structural defects and G band for E_{2g} vibration mode of sp^2 carbon domains, respectively. The high D-band intensity of RGO and NG indicates the presence of a large number of defect sites in the graphene layers.³⁷ The G band of NG shifts slightly ($\sim 10 \text{ cm}^{-1}$) to higher wave numbers with respect to that of RGO, which can be ascribed to the formation of p-type doped graphene.³⁸ The I_D/I_G increases from 0.97 for RGO to 0.98, 0.99 and 1.0 for NGasp, NGgly and NGarg, respectively, which suggests that more defects are formed during the doping of GO.

In order to characterize the exposed surface areas and pore structure of the samples, low-temperature nitrogen physisorption measurements were conducted. Fig. 4c shows the N_2 adsorption-desorption isotherms of freeze-dried RGO, NGasp, NGgly and

NGarg. For RGO, NGgly and NGasp, the profiles are characterized by type IV isotherms with a H2-type hysteresis loop, indicating the presence of mesopores. However, NGarg curves are characterized by type II isotherms with no hysteresis loops. The BET surface area (S_{BET}) of RGO, NGasp, NGgly and NGarg were summarized in Table 2. The S_{BET} of RGO is $352.9 \text{ m}^2 \text{ g}^{-1}$, which is higher than hydrothermally reduced graphene oxide ($265.2 \text{ m}^2 \text{ g}^{-1}$)^[33] in acid medium and lower than hydrazine-reduction graphene oxide ($\sim 487 \text{ m}^2 \text{ g}^{-1}$).^[39] The S_{BET} and total pore volume of NGasp are $367.1 \text{ m}^2 \text{ g}^{-1}$ and $0.24 \text{ cm}^3 \text{ g}^{-1}$, and the corresponding pore size distribution determined by the Barrett–Joyner–Halenda (BJH) method is about 2.6 nm (Fig. 4d). The S_{BET} of NGgly ($207.3 \text{ m}^2 \text{ g}^{-1}$) is lower than that of NGasp. The S_{BET} of $10.5 \text{ m}^2 \text{ g}^{-1}$ of NGarg is significantly lower than those of the other samples, which is consistent with the serious agglomeration of NGarg as disclosed by SEM studies (Fig. 2d).

X-ray photoelectron spectroscopic was carried out to evaluate the surface chemical composition of the samples. The XPS survey spectra of NG and RGO samples are displayed in Fig. 5a. All the spectra show a predominant graphitic C 1s peak at 284.4 eV. After nitrogen doping using amino acid, the intensity of O 1s peak ($\sim 532.4 \text{ eV}$) decreased, and N 1s peak at about 400 eV appeared, which demonstrates the successful incorporation of nitrogen. The N1s peak of NGarg is much stronger than that of NGasp and NGgly, which indicates that the nitrogen content of NGarg is significantly higher than that of the other samples.

A quantitative analysis was performed based on the XPS, and the surface atomic concentrations of C, O, and N were derived from the corresponding peak areas of the XPS and were summarized in Table 3. Compared with RGO, nitrogen doping is accompanied by the reduction of GO after the addition of the three amino acids, as can be proved by the decrease of oxygen content and increase in C/O atomic ratio in NGasp, NGgly and NGarg (Table 3). After hydrothermal reaction of GO using amino acids, the percentage of doped nitrogen was 1.0, 3.0 and 8.9 atom% for NGasp, NGgly and NGarg, respectively. The difference in nitrogen content is largely due to the big differences of mass fraction of nitrogen element in each amino acid (10.5% for aspartic acid, 18.6% for glycine and 32.1% for arginine). The interaction between amino acid and GO might also affect the nitrogen content of NG samples. Arginine (basic) has more positive charges than aspartic acid (acidic). Hence, a stronger interaction of arginine with GO can be expected, which could result in a high nitrogen content of NGarg after hydrothermal reaction. In addition, increase in the amount of DL-aspartic acid improves the nitrogen content from 0.9% (a mass ratio of 1:1) to 1.2% (a mass ratio of 10:1), which suggests that increase the mass ratio cannot improve the nitrogen content significantly (Fig S4†, Table S2†).

Fig. 5b–d show the N 1s region spectra of the samples NGasp, NGgly and NGarg, respectively. The N 1s spectra of all NG samples were decomposed into three peaks: a low binding energy component (N1) at 398.6 - 398.9 eV and two higher binding energy components (N2 and N3) at 399.8 - 400.0 eV and 401.4 - 401.6 eV, respectively. It is known that pyridinic-type nitrogen on carbon surfaces appears at about 398.6 eV and

nitrogen in pyrrole group was found to be at 400.3.^{40, 41} The contribution at $401.5 \pm 0.3 \text{ eV}$ has been assigned to various forms of quaternary nitrogen atoms.⁴¹ Thus, the N1 peak at lower binding energy can be assigned to pyridine group, and the N2 peak to pyrrole group. The N3 component can be assigned to quaternary nitrogen atoms. To assess the amount of different types of N-species created on the NG samples surface quantitatively, the relative percentage of different nitrogen types in every NG samples are calculated and plotted in Fig. 5e. It can be seen clearly that in all samples the pyrrolic-type nitrogen predominates and the pyrrolic-type nitrogen content are 0.59, 2.06 and 6.55 atom % in the sample of NGasp, NGgly and NGarg, respectively. Pyridinic- and pyrrolic-type nitrogen have been confirmed to have the enhancing effects on the capacitance due to their pseudocapacitive contributions.^{23, 43} Hence, the enriched pyrrolic-type nitrogen will be beneficial for the capacitance of NG samples.

The difference in chemical composition and microstructure among these materials will have significant impact on their capacitive properties. The above-mentioned results indicate that NGasp could have the best electrochemical performance, and further studies were therefore carried out to verify this hypothesis. Fig. 6a shows the cyclic voltammetry (CV) curves for RGO and NG samples with a scan rate of 10 mV s^{-1} . The curves exhibit an approximately rectangular shape, characteristic of the ideal double-layer capacitor. The loop area of NGasp is the greatest, followed by RGO. NGarg has the smallest area. These results indicate the highest capacitance for NGasp and lowest capacitance for NGarg. Fig. 6b shows the galvanostatic charge and discharge (GCD) curves of the NG samples tested at the current density of 3 A g^{-1} . The curves are linear and represent regularly symmetrical triangle, and the time accomplishing one charge/discharge cycle for NGasp is much longer than that of other NG samples, indicating the highest capacitance for NGasp. The capacitances for all NG samples are following the order of $\text{NGasp} > \text{RGO} > \text{NGgly} > \text{NGarg}$, which is in accordance with those results of CV analysis.

The specific capacitance values are listed in Table 2. It can be clearly seen that the C_{sc} value for NGasp is 246 F g^{-1} at a current density of 3 A g^{-1} , which is higher than that of RGO (201 F g^{-1}) and also much higher than that of NGgly (161 F g^{-1}) and NGarg (105 F g^{-1}). The CV curves (Fig. S6a†) of NGasp samples exhibit approximately rectangular shapes, characteristic of the double-layer capacitor. The GCD curves at different current densities are displayed in Fig. S6b†, the nearly triangular charge-discharge curves reflect the good capacitive performances of the NGasp. Fig. 6c presents the specific capacitance plots of RGO and NG samples, it can be seen that the C_{sc} value of NGasp is 388 F g^{-1} at current density of 0.5 A g^{-1} , and the value of NGasp is still as high as 219 F g^{-1} even at a high current density of 10 A g^{-1} . Moreover, capacitance retention of 92% (227 F g^{-1} , at 3 A g^{-1}) was obtained after 1000 cycles of charge and discharge (inset of Fig. 6c). The SEM and BET results show that RGO and NGasp have similar morphologies and specific surface area. However, the capacitance of NGasp is higher than that of RGO, which suggests that the sample's electrochem performance can be

enhanced through nitrogen doping. Even though NGgly and NGarg have higher nitrogen level, their specific surface areas are much smaller due to serious agglomeration. Therefore, the total number of effective nitrogen species contributing to the pseudo-capacitance is less than that of NGasp, which is the main reason for lower capacitance of NGgly and NGarg.

Furthermore, the capacitive performance of the samples prepared by adding the other six amino acids was also tested. As shown in Fig. 7, the C_{sc} value of samples by the addition of DL-Aspartic Acid (acidic), L-Glutamic Acid (acidic), L-Leucine (neutral), L-Alanine (neutral), L-Threonine (neutral), L-Glycine (neutral), L-Lysine (basic), L-Histidine (basic) and L-Arginine (basic) are 246, 218, 210, 185, 185, 161, 159, 131 and 105 F g⁻¹, respectively. It is obviously that the specific capacitance of the samples prepared by adding acidic amino acids is higher than that of the samples prepared by using neutral and basic amino acids. The specific capacitance of all samples are following the order of acidic amino acids > neutral amino acids > basic amino acids. As is mentioned above, the charge of amino acid (positively or negatively charged) influences the electrostatic interaction with GO layers, which leads to different morphology of samples, and ultimately different electrochemical performance.

In order to confirm our assumption that the positively (pH < pI) or negatively (pH > pI) charged amino acid affect the morphology of NG and ultimately affect the electrochemical capacitance, additional NG samples were prepared by the same hydrothermal treatment of the previously mixed solutions of GO and amino acid (DL-aspartic acid, L-glycine and L-arginine). The pH of the mixed solution was adjusted with HCl (0.1M) or NaOH (0.1M). After hydrothermal reaction, the products were labeled as NGasp (pH=2), NGgly (pH=7) and NGarg (pH=13), respectively. Electrochemical measurements of the products were performed after purification and the results were listed in Table 4 and shown in Fig. S7†. The nature of the charged amino acid can be changed by adjusting the pH of the mixed solution. The positively charged glycine and arginine (pH < pI) induced GO aggregation through electrostatic repulsion. Hence, low specific capacitance (171 F g⁻¹ and 132 F g⁻¹ at 1 A g⁻¹, respectively) of the previous prepared NGgly and NGarg were obtained. On the contrary, after adjusting the pH of the mixed solution of GO with glycine and arginine to 7 and 13, respectively, the negatively charged ones (pH > pI) enhanced the repulsive force between GO layer. As expected, the as prepared NGgly (pH=7) and NGarg (pH=13) exhibit higher specific capacitance of 253 F g⁻¹ and 191 F g⁻¹ at 1 A g⁻¹, respectively. However, the specific capacitance of NGasp (pH=2) is still higher than that of NGasp, although the pH value is lower than the pI of aspartic acid (pH < pI). Recently, Alshareef et al.^[33] reported that hydrothermally reduced graphene oxide (RGO) produced under acidic conditions shown higher specific capacitance than basic conditions, because acidic media yield RGO with more oxygen-functional groups, which could provide additional pseudocapacitance. Hence, the higher specific capacitance of NGasp (pH=2) may be caused by pseudocapacitance contribution. The additional pseudocapacitance can be attributed to more oxygen-functionalities in more acidic condition.

Electrochemical impedance spectroscopy (EIS) is a useful measurement that gives some information regarding internal resistance of the electrode material and resistance between the electrode and electrolyte. It is well accepted that a semicircle reflects the electrochemical reaction impedance of the electrode, and a smaller semicircle means smaller charge transfer resistance.⁴⁴ It can be clearly seen from Fig. 6d that the charge transfer resistance for NGasp was the lowest among all samples. In contrast, the resistance of NGarg was the largest. In addition, NGasp showed the steepest slope of the plot, which indicates that NGasp had the lowest charge-transfer resistance and excellent conductivity.

The above-mentioned results show that NGasp exhibits better capacitive behavior, which can be related to the continuous 3D network structure and large specific surface area. The porous network and flatter graphene structure led to the fast adsorption and diffusion of the potassium ion on the electrode surface, so that a very high specific capacity can be obtained. The positively charged L-glycine and L-arginine induce the aggregation of NGgly and NGarg samples through electrostatic attraction. Consequently, low capacitances are obtained. Furthermore, the nitrogen-doping led to the formation of different nitrogen groups dominating by pyrrolic N, which is known to provide pseudo-capacitance. Even though NGasp has the lowest nitrogen level, the total number of effective nitrogen species contributing to the pseudo-capacitance is more than the other two samples due to its largest specific surface area. Hence, the electrochemical properties of NG samples strongly depend on the proper 3D network structure and large specific surface area, and effective nitrogen content as well.

4. Conclusions

In summary, NG samples were synthesized by a simple one-pot hydrothermal process using graphene oxide and three kinds of amino acids with different acidities. Acidic amino acid yield NG with cross-linked 3D network and a large surface area of 367.1 m² g⁻¹ (NGasp), while the obtained NG from basic amino acid shows a tightly stacked structure and a much smaller surface area of 10.5 m² g⁻¹ (NGarg). The negatively charged acidic amino acid (pH > pI) can prevent GO flakes from aggregation through electrostatic attraction, whereas the neutral and basic amino acids with positive charges (pH < pI) induce GO aggregation through electrostatic repulsion. Hence, the electrostatic interaction is behind the differences in morphology and specific surface area of the obtained NG samples. XPS confirmed the doping of nitrogen with pyrrolic nitrogen as dominating nitrogen species. The surface N content of NGasp is much lower (1.0 at%) than that of NGgly (3.0 at%) and NGarg (8.9 at%). However, the effective nitrogen content of NGasp contributing to the pseudo-capacitance is more than that of NGgly and NGarg due to its 3D network and large surface area. Hence, NGasp exhibits the highest electrochemical capacitance of 246 F g⁻¹ at 3 A g⁻¹ and 388 F g⁻¹ at 0.5 A g⁻¹. The specific capacitance for the nine samples are following the order of acidic amino acids > neutral amino acids > basic amino acids. The microstructure, surface area and effective

nitrogen content play important roles in the capacitive performance of the NG samples.

Acknowledgements

This research was financially supported by the National Natural Science Foundation of China (No. U1203292, 21271151 and 21361024), and the Xinjiang Autonomous Region of major projects: (No. 201130113-1).

Notes and references

^aKey Laboratory of Material and Technology for Clean Energy, Ministry of Education, Key Laboratory of Advanced Functional Materials, Autonomous Region, Institute of Applied Chemistry, Xinjiang University, 830046 Xinjiang, P. R. China.

Fax: +86-991- 8588883; Tel: +86-991-8583083; E-mail: jdz@xju.edu.cn

^bLaboratory of Industrial Chemistry, Ruhr-University Bochum, 44780

Bochum, Germany.

† Dedicated to Professor Xinquan Xin on the occasion of his 80th birthday.

‡ Electronic Supplementary Information (ESI) available: Extensive experimental characterization details of NG, NGasp1, NGasp10 and other six amino acids, concerning FT-IR, SEM, XRD, Raman and XPS spectroscopy and electrochemical measurements.

1 Y. W. Zhu, S. Murali, W. W. Cai, X. S. Li, J. W. Suk, J. R. Potts and R. S. Ruoff, *Adv. Mater.*, 2010, **22**, 3906-3924.

2 P. Ayala, R. Arenal, M. Rummeli, A. Rubio and T. Pichler, *Carbon*, 2010, **48**, 575-586.

3 Z. S. Wu, W. C. Ren, L. Xu, F. Li and H. M. Cheng, *ACS Nano*, 2011, **5**, 5463-5471.

4 Y. Zhao, C. G. Hu, Y. Hu, H. H. Cheng, G. Q. Shi and L. T. Qu, *Angew. Chem. Int. Ed.*, 2012, **51**, 11371-11375.

5 C. H. Choi, M. W. Chung, H. C. Kwon, S. H. Park and S. I. Woo, *J. Mater. Chem. A*, 2013, **1**, 3694-3699.

6 S. U. Lee, R. V. Belosludov, H. Mizuseki and Y. Kawazoe, *Small*, 2009, **5**, 1769-1775.

7 D. Usachov, O. Vilkov, A. Gruneis, D. Haberer, A. Fedorov, V. K. Adamchuk, A. B. Preobrajenski, P. Dudin, A. Barinov, M. Oehzelt, C. Laubschat and D. V. Vyalikh, *Nano Lett.*, 2011, **11**, 5401-5407.

8 H. T. Liu, Y. Q. Liu and D. B. Zhu, *J. Mater. Chem.*, 2011, **21**, 3335-3345.

9 N. Li, Z. Y. Wang, K. K. Zhao, Z. J. Shi, Z. N. Gu and S. K. Xu, *Carbon*, 2010, **48**, 255-259.

10 R. I. Jafri, N. Rajalakshmi and S. Ramaprabhu, *J. Mater. Chem.*, 2010, **20**, 7114-7117.

11 H. M. Jeong, J. W. Lee, W. H. Shin, Y. J. Choi, H. J. Shin, J. K. Kang and J. W. Choi, *Nano Lett.*, 2011, **11**, 2472-2477.

12 D. C. Wei, Y. Q. Liu, Y. Wang, H. L. Zhang, L. P. Huang and G. Yu, *Nano Lett.*, 2009, **9**, 1752-1758.

13 Z. Jin, J. Yao, C. Kittrell and J. M. Tour, *ACS Nano*, 2011, **5**, 4112-4117.

14 C. H. Zhang, L. Fu, N. Liu, M. H. Liu, Y. Y. Wang and Z. F. Liu, *Adv. Mater.*, 2011, **23**, 1020-1024.

15 Z. H. Sheng, L. Shao, J. J. Chen, W. J. Bao, F. B. Wang and X. H. Xia, *ACS Nano*, 2011, **5**, 4350-4358.

16 X. R. Wang, X. L. Li, L. Zhang, Y. K. Yoon, P. K. Weber, H. L. Wang, J. Guo and H. J. Dai, *Science*, 2009, **324**, 768-771.

17 Y. X. Xu, K. X. Sheng, C. Li and G. Q. Shi, *ACS nano*, 2010, **4**, 4324-4330.

18 G. Wang, L. T. Jia, Y. Zhu, B. Hou, D. B. Li and Y. H. Sun, *RSC Adv.*, 2012, **2**, 11249-11252.

19 P. Chen, J. J. Yang, S. S. Li, Z. Wang, T. Y. Xiao, Y. H. Qian and S. H. Yu, *Nano Energy*, 2013, **2**, 249-256.

20 Y. Lu, F. Zhang, T. Zhang, K. Leng, L. Zhang, X. Yang, Y. Ma, Y. Huang, M. Zhang and Y. Chen, *Carbon*, 2013, **63**, 508-516.

21 J. W. Lee, J. M. Ko and J. D. Kim, *Electrochim. Acta.*, 2012, **85**, 459-466.

22 H. L. Guo, P. Su, X. F. Kang and S. K. Ning, *J. Mater. Chem. A*, 2013, **1**, 2248-2255.

23 L. Sun, L. Wang, C. G. Tian, T. X. Tan, Y. Xie, K. Y. Shi, M. T. Li and H. G. Fu, *RSC Adv.*, 2012, **2**, 4498-4506.

24 J. J. Wu, D. Zhang, Y. Wang and B. R. Hou, *J. Power Sources.*, 2013, **227**, 185-190.

25 D. H. Long, W. Li, L. C. Ling, J. Miyawaki, I. Mochida and S. H. Yoon, *Langmuir*, 2010, **26**, 16096-16102.

26 X. Q. An, J. C. Yu, F. Wang, C. H. Li and Y. C. Li, *Appl. Catal. B: Environ.*, 2013, **129**, 80-88.

27 G. P. Hao, W. C. Li, S. Wang, G. H. Wang, L. Qi and A. H. Lu, *Carbon*, 2011, **49**, 3762-3772.

28 S. A. Wohlgemuth, F. Vilela, M. M. Titirici and M. Antonietti, *Green Chem.*, 2012, **14**, 741-749.

29 Y. W. Zhang, J. Q. Tian, H. Y. Li, L. Wang, X. Y. Qin, A. M. Asiri, A. O. Al-Youbi and X. P. Sun, *Langmuir*, 2012, **28**, 12893-12900.

30 C. H. Choi, S. Hyeon Park and S. I. Woo, *Green Chem.*, 2011, **13**, 406-412.

31 D. Z. Chen, L. D. Li and L. Guo, *Nanotechnology*, 2011, **22**, 325601-325607.

32 Y. Zhou, Q. Bao, L. A. L. Tang, Y. Zhong and K. P. Loh, *Chem. Mater.*, 2009, **21**, 2950-2956.

33 Y. C. Bai, R. B. Rakhi, W. Chen and H. N. Alshareef, *J. Power Sources*, 2013, **233**, 313-319.

34 C. B. Navarro, E. Coronado, C. Martí-Gastaldo, J. F. Sánchez-Royo and M. G. Gómez, *Nanoscale*, 2012, **4**, 3977-3982.

35 D. C. Marcano, D. V. Kosynkin, J. M. Berlin, A. Sinitskii, Z. Sun, A. Slesarev, L. B. Alemany, W. Lu and J. M. Tour, *ACS Nano*, 2010, **4**, 4806-4814.

36 D. Li, M. B. Müller, S. Gilje, R. B. Kaner and G. G. Wallace, *Nat. Nanotechnol.*, 2008, **3**, 101-105.

37 D. S. Geng, S. L. Yang, Y. Zhang, J. L. Yang, J. Liu, R. Y. Li, T. K. Sham, X. L. Sun, S. Y. Ye and S. Knights, *Appl. Surf. Sci.*, 2011, **257**, 9193-9198.

38 D. H. Deng, X. L. Pan, L. Yu, Y. Cui, Y. P. Jiang, J. Qi, W. X. Li, Q. Fu, X. C. Ma, Q. K. Xue, G. Q. Sun and X. H. Bao, *Chem. Mater.*, 2011, **23**, 1188-1193.

39 S. Park, J. An, J. R. Potts, A. Velamakanni, S. Murali and R. S. Ruoff, *Carbon*, 2011, **49**, 3019-3023.

40 S. Kundu, W. Xia, W. Busser, M. Becker, D. A. Schmidt, M. Havenith and M. Muhler, *Phys. Chem. Chem. Phys.*, 2010, **12**, 4351-4359.

41 C. Li, A. Q. Zhao, W. Xia, C. H. Liang and Martin Muhler, *J. Phys. Chem. C*, 2012, **116**, 20930-20936.

42 J. R. Pels, F. Kapteijn, J. A. Moulijn, Q. Zhu and K. M. Thomas, *Carbon*, 1995, **33**, 1641-1653.

43 D. H. Jurcakova, M. Seredych, G. Q. Lu and T. J. Bandosz, *Adv. Funct. Mater.*, 2009, **19**, 438-447.

44 L. F. Chen, X. D. Zhang, H. W. Liang and M. G. Kong, *ACS Nano*, 2012, **6**, 7092-7102.

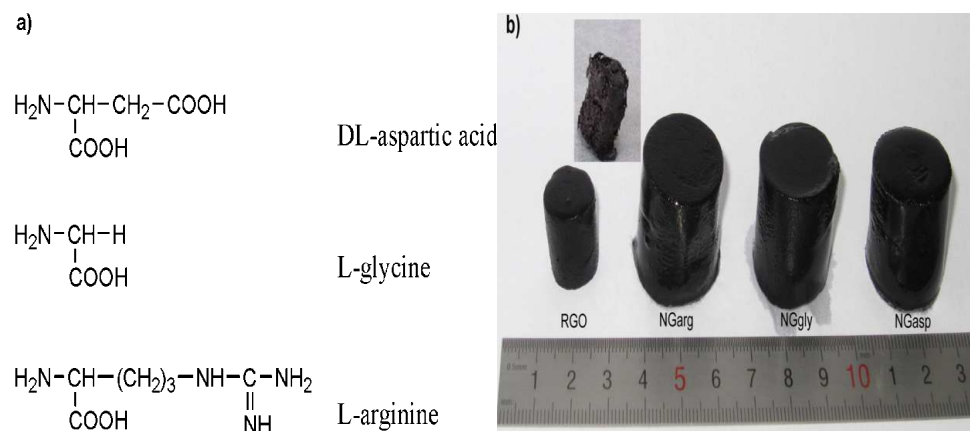


Fig. 1 (a) Selected three typical amino acids as the doping agents and (b) Photographs of typical RGO and NG, inset shows the typical NG after freeze-dried.

5

10

15

20

25

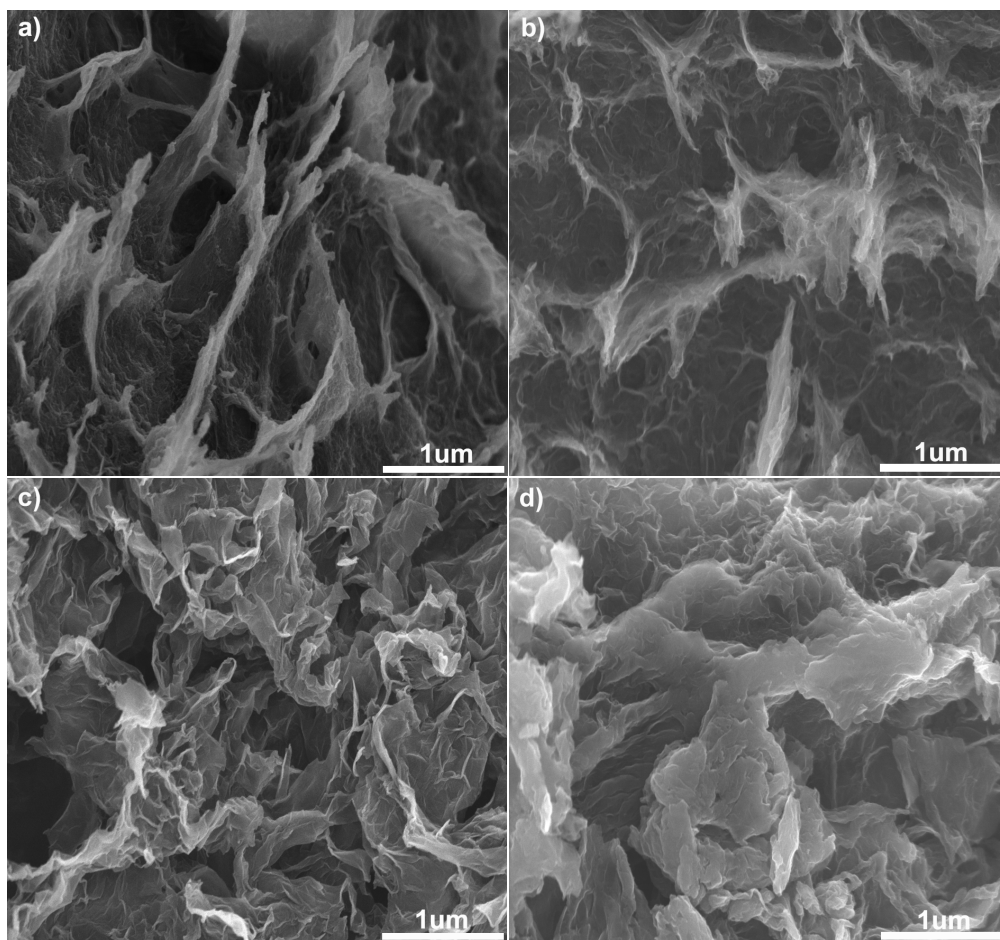


Fig. 2 (a) SEM images of RGO; (b-d) SEM images of NGasp, NGgly and NGarg, respectively.

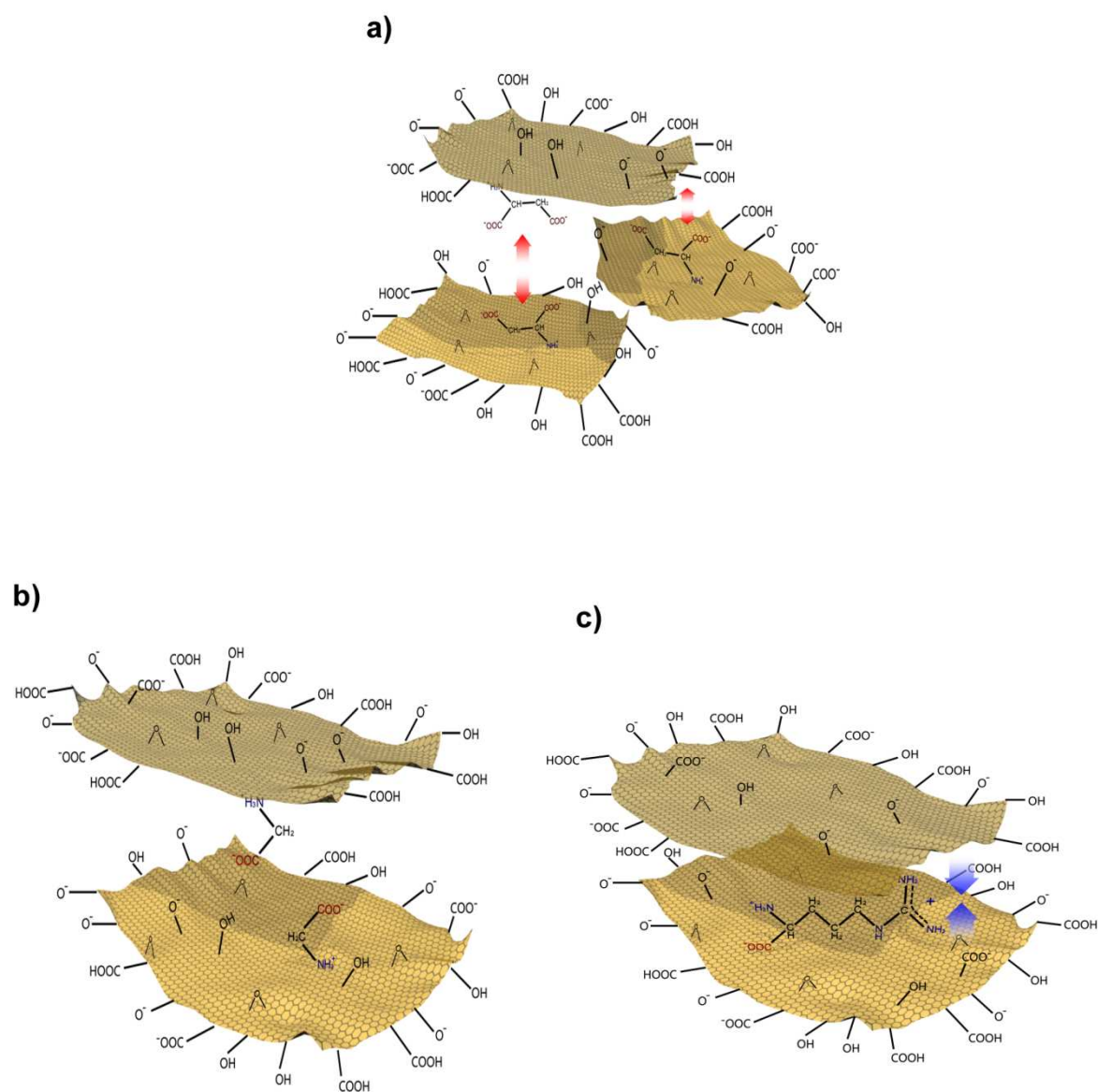


Fig. 3 Probably interaction between amino acids and GO. (a) DL-aspartic acid with GO, (b) L-glycine with GO and (c) L-arginine with GO.

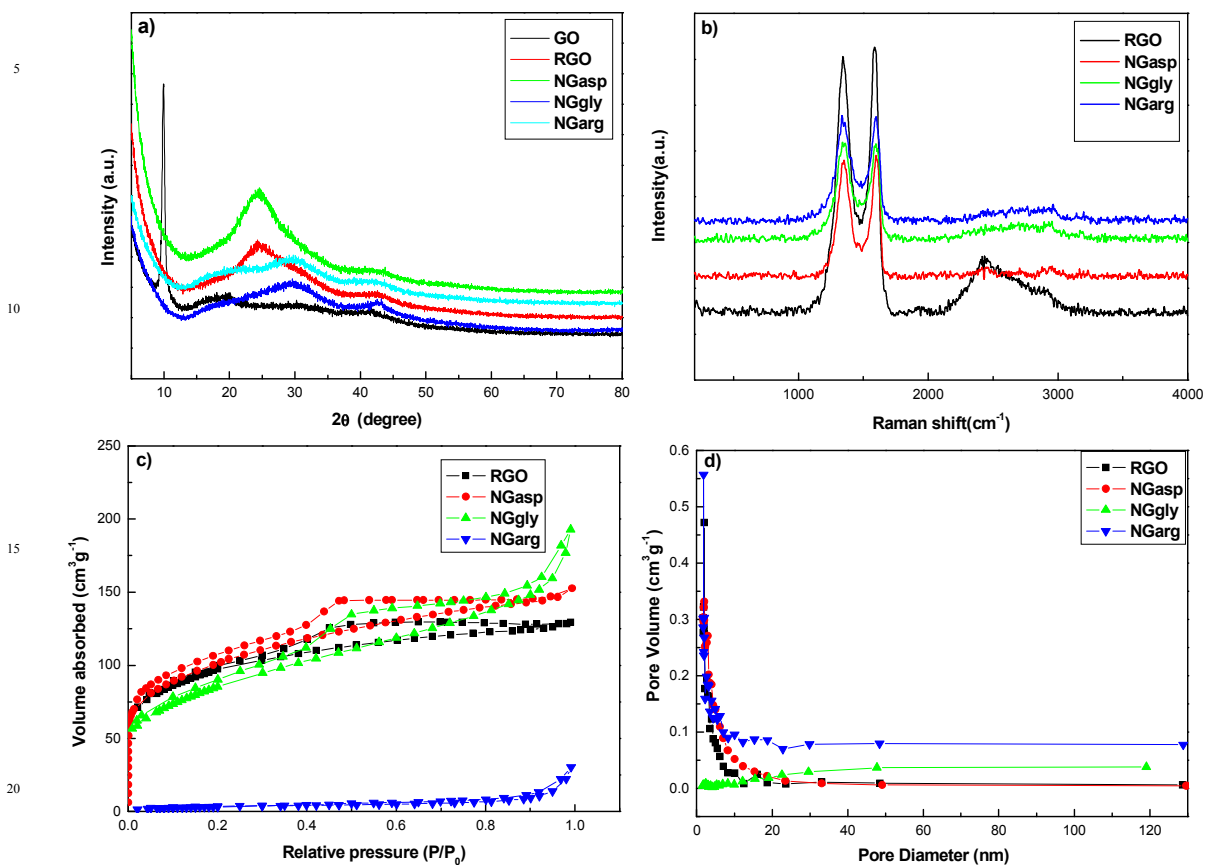


Fig. 4 (a) XRD patterns of GO, RGO and NG samples. (b) Raman spectra, (c) N_2 adsorption-desorption isotherms and (d) pore size distribution of RGO, NGasp, NGgly and NGarg, respectively.

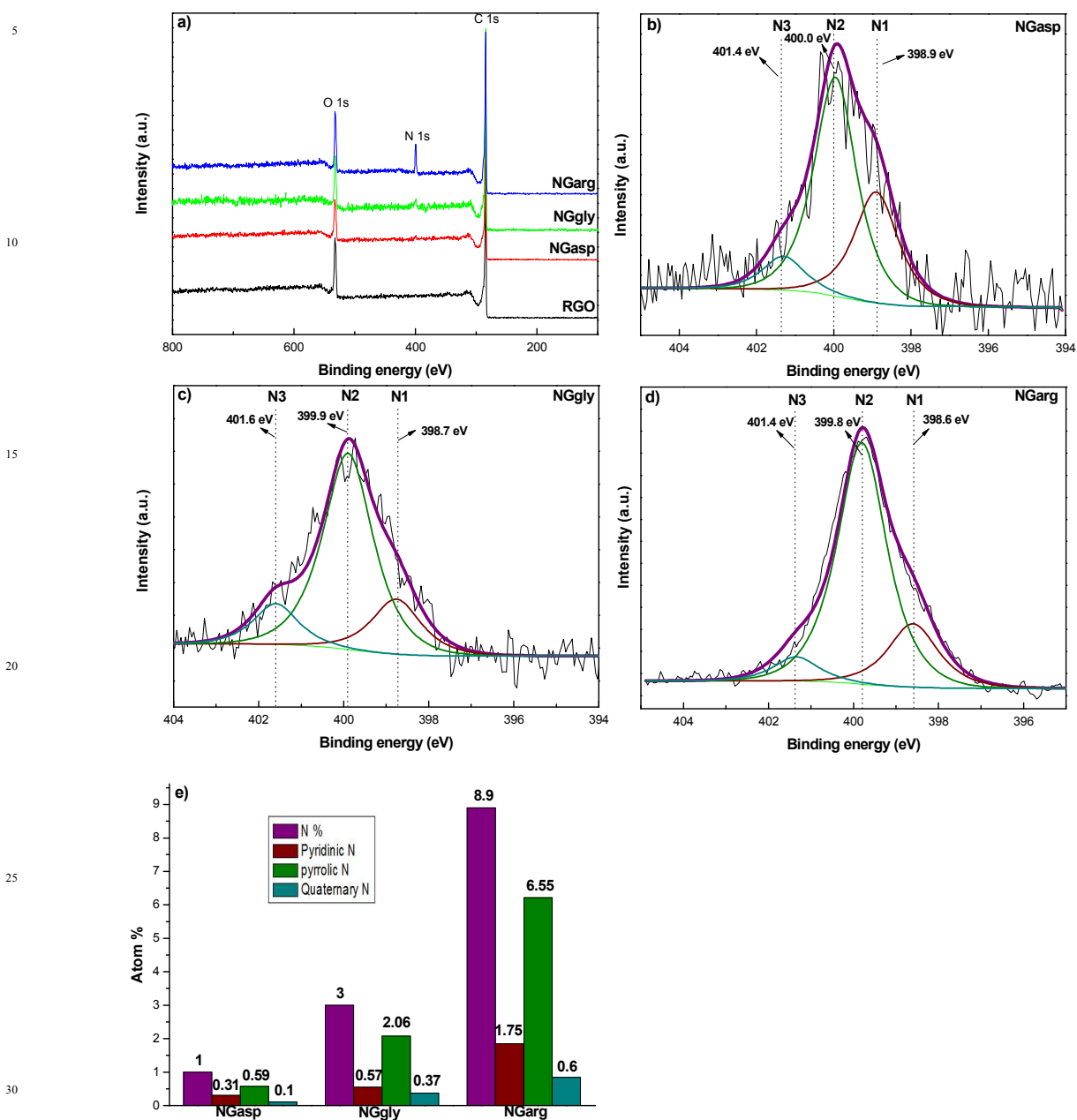


Fig. 5 (a) XPS spectra for RGO and NG samples; (b), (c) and (d) N 1s region spectra of the samples NGasp, NGgly and NGarg; (e) is atomic% of nitrogen in every NG sample and its associated resolved components in atom%. The purple bar is the total atomic% of nitrogen in that sample.

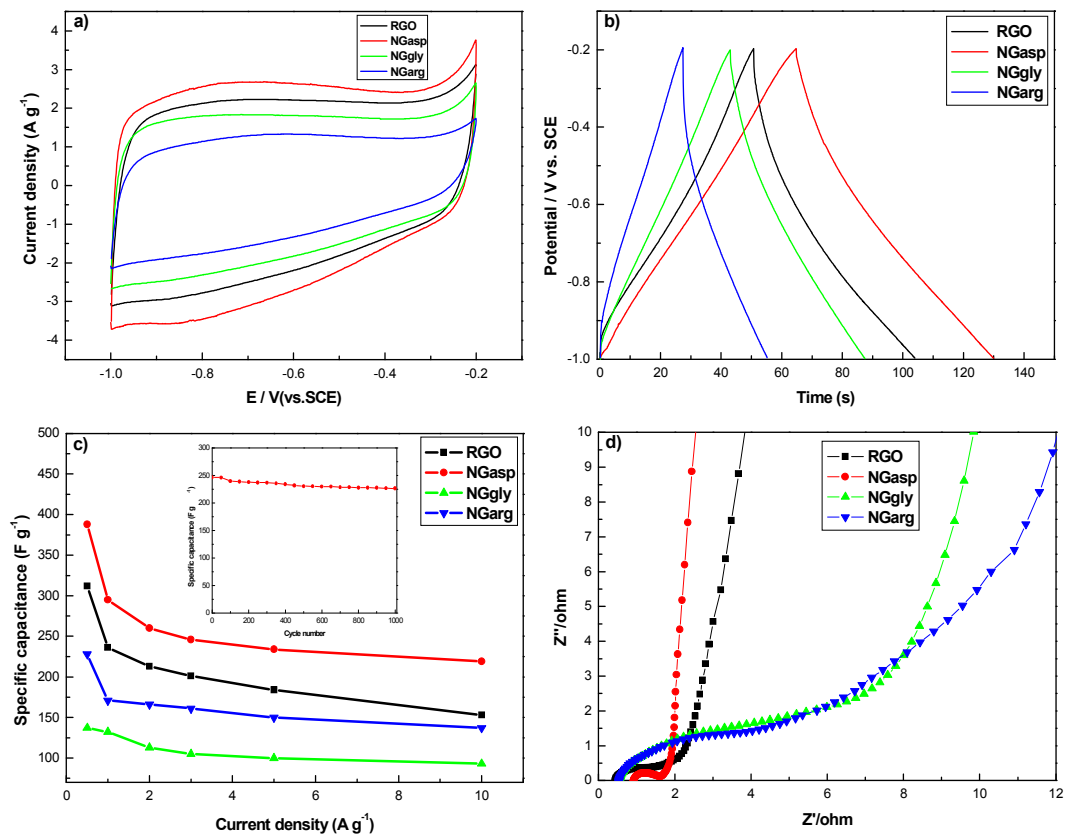


Fig. 6 (a) CV curves measured at 10 mV s⁻¹, (b) GCD curves tested at current density of 3 A g⁻¹, (c) relationship of the specific capacitance with respect to the current density (inset: variations of specific capacitance versus cycle number of NGasp at a current density of 3 A g⁻¹) and (d) Nyquist plots for RGO, NGasp, NGgly and NGarg, respectively.

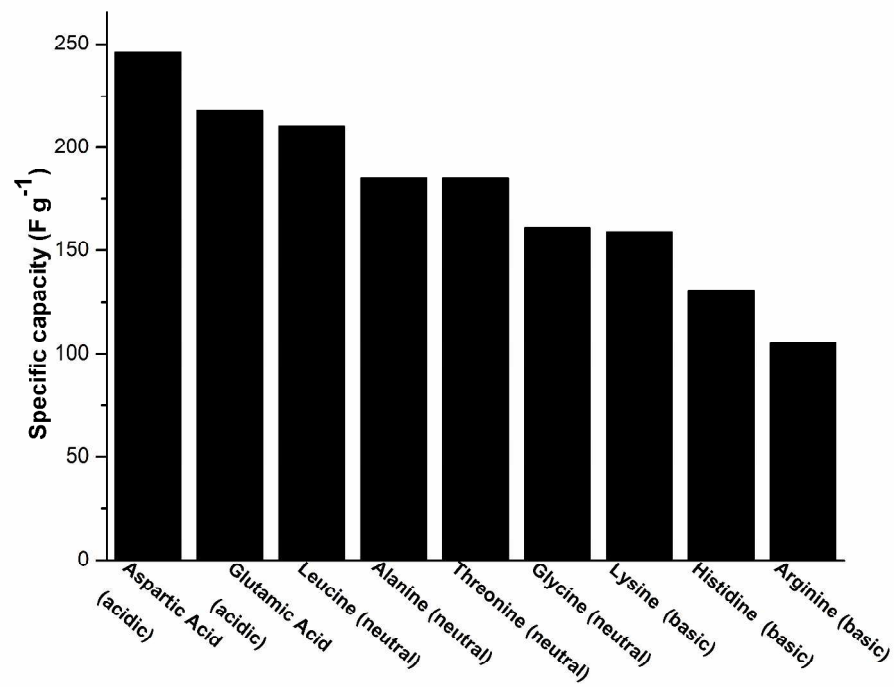


Fig. 7 Specific capacitance values of the samples that addition of different amino acids, tested at the current density of 3 A g⁻¹.

5

10

15

20

Table 1 The pH value of GO with different amino acids, pI of the nine amino acids .

Amino acids	pH	pI	pH Vs. pI
Aspartic Acid (acidic)	3.2	2.97	pH > PI
Glutamic Acid (acidic)	3.4	3.22	pH > PI
Leucine (neutral)	3.6	5.98	pH < PI
Alanine (neutral)	3.8	6.00	pH < PI
Threonine (neutral)	3.5	6.16	pH < PI
Glycine (neutral)	4.1	5.97	pH < PI
Lysine (basic)	2.8	9.74	pH < PI
Histidine (basic)	7.3	7.59	pH < PI
Arginine (basic)	8.4	10.76	pH < PI

Table 2 List of parameters deduced from XRD data, BET and specific capacitances for different samples.

Samples	$2\theta(^{\circ})$	$d(\text{nm})^a$	BET($\text{m}^2 \text{g}^{-1}$)	$C_{sc} (\text{F g}^{-1})$	
				(3 A g^{-1})	(0.5 A g^{-1})
GO	9.90	0.890			
RGO	24.72	0.360	352.9	201	279
NGasp	24.53	0.364	367.1	246	388
NGgly	29.59	0.301	207.3	161	228
NGarg	29.91	0.300	10.5	105	137

^aThe Bragg equation, $n\lambda = 2d \sin\theta$ was used for the calculation, where n is an integer, λ is the wavelength of the incident wave (Cu α radiation, $\lambda = 1.5418 \text{ \AA}$), d is the spacing between the planes in the atomic lattice, and θ is the angle between the incident ray and the scattering planes.

Table 3 The relative surface concentrations of C, O, N and C/O atomic ratio of RGO and NG samples by XPS analyses.

Samples	$C_{\text{XPS}}(\text{at.}\%)$	$O_{\text{XPS}}(\text{at.}\%)$	$N_{\text{XPS}}(\text{at.}\%)$	C/O
RGO	83.7	16.3		5.1
NGasp	86.2	12.8	1.0	6.7
NGgly	82.7	14.3	3.0	5.8
NGarg	77.0	14.1	8.9	5.5

Table 4 The nature of charge for the three amino acids and the specific capacitances of the produced NG under different pH.

Amino acid	pH (the mixture of GO and amino acid)	pI	pH Vs. pI	Charge	C _{sc} (F g ⁻¹) of NG at 1A g ⁻¹
Aspartic Acid	3.2	2.97	pH > pI	negative	295
	2.0		pH < pI	positive	348
Glycine	4.1	5.97	pH < pI	positive	171
	7.0		pH > pI	negative	253
Arginine	8.4	10.76	pH < pI	positive	132
	13.0		pH > pI	negative	191

10

40

15

45

20

50

25